

An Integrated Groundwater Model using Multicomponent Multiphase Theory (II) - Numerical Analysis and Model Applications -

Joon-Hyun Kim* and Michael K. Stenstrom**

* Environmental Engineering Department Kangwon National University

** Civil and Environmental Engineering Department University of California, Los Angeles

ABSTRACT

A multidimensional finite element code is developed for the integrated groundwater model in the companion paper, with provisions for complex transport and transformation processes. The FORTRAN code with dynamic array allocation, is sufficiently flexible to work across a wide spectrum of computers, including an IBM ES 9000/900 vector facility, Unix workstations and PCs, for one-, two- and three-dimensional problems. To reduce the computation time and storage requirements, the system equations are decoupled and solved using a banded global matrix solver, with the vector and parallel processing on the IBM 9000. To avoid the numerical oscillations of the nonlinear problems in the case of convective dominant transport, the techniques of upstream weighting, mass lumping, and elementary-wise parameter evaluation are applied. The instability and convergence criteria of the nonlinear problems are studied. The model is highly structured to facilitate the inclusion of the additional constitutive and reaction equations. The model can simulate the transport and transformation of a complex mixture of groundwater contaminants (e.g., a mixture of light and heavy hydrocarbons, water-borne contaminants and volatile contaminants). To demonstrate the model's robustness, several hypothetical problems, from traditional groundwater flow to multicomponent multiphase flow, are simulated through parameter substitution. The cases presented are unsaturated flow through an embankment, one-, two-, three-dimensional multiphase flow, and three dimensional composite multiphase TCE migration. Parameter dependency and sensitivity of the model are analyzed with respect to the boundary conditions, the fluid conductivity, and the magnitude of contaminant source.

INTRODUCTION

The accompanying paper [Kim and Stenstrom, this issue] reviewed previous literature on composite groundwater modeling and developed an integrated groundwater model using a compact notation. This paper describes a numerical method to solve the governing equations, which is broadly applicable to a variety of problems and computing platform. A brief review of previous groundwater modeling efforts is presented to provide background and support as follows: 1) finite difference models, 2) finite element models, 3) front tracking models including the Eulerian-Lagrangian method, 4) boundary element models, 5) analytical solutions, and 6) vector and parallel processing. The developed numerical model is verified for a broad range of system parameters, using literature data. Extensive parameter and experimental studies are in preparation, and will be presented later.

NUMERICAL ANALYSIS

The comprehensive governing equation of the integrated model was presented as follows [Kim and Stenstrom, this issue] :

$$\begin{aligned} & \sum_{\alpha=1}^3 \left[\sum_{\beta=1}^3 (\rho_{\beta} w_{\beta}^i S_{\beta\alpha}) \frac{\partial h_{\alpha}}{\partial t} + \phi \rho_{\alpha} w_{\alpha}^i \frac{\partial S_{\alpha}}{\partial t} + \phi S_{\alpha} \rho_{\alpha} \frac{\partial w_{\alpha}^i}{\partial t} \right] + \frac{\partial}{\partial t} ((1-\phi) \rho_s w_s^i) \\ & = \sum_{\alpha=1}^3 \left[\nabla \cdot \left(\rho_{\alpha} w_{\alpha}^i K_{\alpha} \left(\nabla h_{\alpha} + \frac{\rho_{\alpha}}{\rho_w} \mathbf{j} \right) \right) + \nabla \cdot (\phi S_{\alpha} D_{\alpha}^i \nabla (\rho_{\alpha} w_{\alpha}^i)) + \phi S_{\alpha} (J_{\alpha}^i + g_{\alpha}^i) \right] \quad (1) \end{aligned}$$

To solve the equation (1), the weighted residual form is derived by applying the asymmetric weighting function w_i and integrating over the spatial domain as shown in equation (2).

$$\sum_{\alpha=1}^3 \left[\int w_i \sum_{\beta=1}^3 (\rho_{\beta} w_{\beta}^i S_{\beta\alpha}) \frac{\partial h_{\alpha}}{\partial t} dR + \int w_i \phi \rho_{\alpha} w_{\alpha}^i \frac{\partial S_{\alpha}}{\partial t} dR + \int w_i \phi S_{\alpha} \rho_{\alpha} \frac{\partial w_{\alpha}^i}{\partial t} dR \right] + \int w_i \frac{\partial}{\partial t} ((1-\phi) \rho_s w_s^i) dR$$

$$= \sum_{\alpha=1}^3 \left[\int W_i \nabla (\rho_\alpha w_\alpha^j K_\alpha) \left(\nabla h_\alpha + \frac{\rho_\alpha}{\rho_w} \vec{j} \right) dR + \int W_i \nabla (\phi S_\alpha D_\alpha^j \nabla (\rho_\alpha w_\alpha^j)) dR + \int W_i \phi S_\alpha (I_\alpha^j + g_\alpha^j) dR \right] \quad (2)$$

Due to the complex form of equation (2), integrated element matrices are defined as follows :

$$[EM_{i,j}] = \langle W_i, N_j \rangle, [EV_{jd,j,j}] = \langle W_i, \frac{dN_j}{dx_{jd}} \rangle, [EK_{jd,j,j}] = \langle \frac{dW_i}{dx_{jd}}, N_j \rangle, [ED_{jd,jd,j,j}] = \langle \frac{dW_i}{dx_{jd}}, \frac{dN_j}{dx_{jd}} \rangle \quad (3)$$

where, N_j is basis function of node j , W_i is weighting function of node i , id, jd are indices for spatial directions ($1=x, 2=y, 3=z$). The basis function only depends upon the geometry of each element; therefore, the evaluation of the basis function needs to be performed only once, which greatly reduces computation time. All the basis functions are evaluated at all Gaussian points and later assembled when the integration of element matrices is performed. By mapping, the integration is performed in the local domain. The linear basis functions in each direction are combined to derive the multi-dimensional bilinear basis functions. Asymmetric weighting functions are developed from the basis function by adding asymmetric weighting terms [Huyakorn and Nikuha, 1979]. Numerical integrations is implemented at Gaussian points. Thus, nodal parameter values should be changed to element-wise parameter values using the basis function $N_{i,jg}$ at Gaussian point ig .

$$(\rho_\beta w_\beta^j S_\beta \alpha) = \sum_{ig=1}^{ng} (\rho_\beta w_\beta^j S_\beta \alpha)_{ig} N_{i,jg} \quad (\rho_\alpha w_\alpha^j K_\alpha)_i = \sum_{ig=1}^{ng} (\rho_\alpha w_\alpha^j K_\alpha)_{ig} N_{i,jg} \quad (\phi S_\alpha \rho_\alpha)_i = \sum_{ig=1}^{ng} (\phi S_\alpha \rho_\alpha)_i N_{i,jg} \quad (4)$$

Where, i is nodal number index, and ng is total number of Gaussian points in each element.

Applying the integrated element matrices, element-wise parameters, and Green's theorem, the weighted residual equation is discretized as follows :

$$\begin{aligned} & \sum_{e=1}^{nel} \left\{ \sum_{j=1}^{nn} \left(\sum_{\alpha=1}^{na} [EM_{i,j}] \left[\sum_{\beta=1}^{na} (\rho_\beta w_\beta^j S_\beta \alpha)_j \right] \frac{\partial h_{\alpha,j}}{\partial x} + (\phi \rho_\alpha w_\alpha^j)_j \frac{\partial S_{\alpha,j}}{\partial x} + (\phi \rho_\alpha S_\alpha)_j \frac{\partial w_{\alpha,j}^j}{\partial x} \right) \right. \\ & \left. + \sum_{id=1}^{nd} \sum_{jd=1}^{nd} \left\{ [ED_{jd,jd,j,j}] (\rho_\alpha w_\alpha^j K_\alpha)_{h_{\alpha,j}} + (\phi S_\alpha \rho_\alpha D_\alpha^j)_j w_{\alpha,j}^j + [EM_{i,j}] \frac{\partial}{\partial x} ((1-\phi) \rho_s w_s^j) \right\} \right. \\ & = \sum_{\alpha=1}^{na} \left\{ \sum_{j=1}^{nn} \left(- \sum_{jd=1}^{nd} [EK_{jd,j,j}] \left(\rho_\alpha w_\alpha^j K_\alpha \frac{\rho_\alpha}{\rho_w} \right)_j \right) + [EM_{i,j}] (\phi S_\alpha (I_\alpha^j + g_\alpha^j)) \right. \\ & \left. + \int W_{ib} \rho_\alpha w_\alpha^j K_\alpha \left(\nabla h_\alpha + \frac{\rho_\alpha}{\rho_w} \vec{j} \right) \cdot \vec{n} dB + \int W_{ib} \phi S_\alpha D_\alpha^j \nabla (\rho_\alpha w_\alpha^j) \cdot \vec{n} dB \right\} \quad (5) \end{aligned}$$

where, nel is total number of elements, nd is dimension of the problem, nn is total number of nodes in each element, and na is total number of phases excluding soil phase.

Total boundary loads of advective and dispersive mass flux are as follows :

$$\int W_i \rho_\alpha w_\alpha^j K_\alpha \left(\nabla h_\alpha + \frac{\rho_\alpha}{\rho_w} \vec{j} \right) \cdot \vec{n} dB = - \int W_i q_{\alpha,h}^j dB \quad (6.1)$$

$$\int W_i \phi S_\alpha D_\alpha^j \nabla (\rho_\alpha w_\alpha^j) \cdot \vec{n} dB = - \int W_i q_{\alpha,d}^j dB \quad (6.2)$$

where, $q_{\alpha,h}^j = -\rho_\alpha w_\alpha^j K_\alpha \left(\nabla h_\alpha + \frac{\rho_\alpha}{\rho_w} \vec{j} \right) \cdot \vec{n}$ is outward normal advective flux, and $q_{\alpha,d}^j = -\phi S_\alpha D_\alpha^j \nabla (\rho_\alpha w_\alpha^j) \cdot \vec{n}$ is outward normal dispersive flux.

Combining the generalized finite difference algorithm along time domain provides the final form of the finite element analogue of the integrated transport equation, as follows :

$$\begin{aligned} & \sum_{e=1}^{nel} \left\{ \sum_{j=1}^{nn} \left(\sum_{\alpha=1}^{na} [EM_{i,j}] \left[\sum_{\beta=1}^{na} (\rho_\beta w_\beta^j S_\beta \alpha)_j (h_{\alpha,j}^{n+1} - h_{\alpha,j}^n) + (\phi \rho_\alpha w_\alpha^j)_j (S_{\alpha,j}^{n+1} - S_{\alpha,j}^n) + (\phi \rho_\alpha S_\alpha)_j (w_{\alpha,j}^{n+1} - w_{\alpha,j}^n) \right] \right) \right. \\ & \left. + \sum_{id=1}^{nd} \sum_{jd=1}^{nd} \left\{ [ED_{jd,jd,j,j}] (\rho_\alpha w_\alpha^j K_\alpha)_j^{n+1} h_{\alpha,j}^{n+1} + (\phi S_\alpha \rho_\alpha D_\alpha^j)_j^{n+1} (w_{\alpha,j}^j)^{n+1} \right. \right. \\ & \left. \left. + (1-\phi) [ED_{jd,jd,j,j}] (\rho_\alpha w_\alpha^j K_\alpha)_j^n h_{\alpha,j}^n + (\phi S_\alpha \rho_\alpha D_\alpha^j)_j^n (w_{\alpha,j}^j)^n \right\} + \frac{1}{\Delta t} [EM_{i,j}] \left\{ ((1-\phi) \rho_s w_s^j)^{n+1} - ((1-\phi) \rho_s w_s^j)^n \right\} \right. \\ & = \sum_{\alpha=1}^{na} \left\{ \sum_{j=1}^{nn} \left[- \sum_{jd=1}^{nd} [EK_{jd,j,j}] \left(\rho_\alpha w_\alpha^j K_\alpha \frac{\rho_\alpha}{\rho_w} \right)_j \right] + [EM_{i,j}] (\phi S_\alpha (I_\alpha^j + g_\alpha^j))_j \right\} - \int W_i q_{\alpha,h}^j dB - \int W_i q_{\alpha,d}^j dB \quad (7) \end{aligned}$$

where, ε is time weighting factor. The boundary flux is integrated as follows using the multidimensional basis functions as follows :

$$f_{\alpha,d,j}^i = \int W_{ib} q_{\alpha,d}^i dB = \sum_{b=1}^{nb} \langle W_{ib}, N_j \rangle q_{\alpha,d,b}^i \quad (8)$$

where, ib is boundary nodal number, nb is total number of boundary nodes, and $f_{\alpha,d,j}^i$ is dispersive boundary load.

To solve the above system with respect to the pressure, saturation and mass fraction terms, the assembled global matrix and load vector of species i in α phase are represented as follows :

$$\{Ah_{\alpha}^i\} = \sum_{\alpha} \sum_j \left[\frac{1}{\Delta t} [EM_{i,j}] \sum_{\beta} (\rho_{\beta} w_{\beta}^i S_{\beta\alpha})_j^{n+1} + \sum_{id} \sum_{jd} \{d[ED]_{id,jd,i,j} K(\rho_{\alpha} w_{\alpha}^i K_{\alpha})_j^{n+1}\} \right] \quad (9.1)$$

$$\{As_{\alpha}^i\} = \sum_{\alpha} \sum_j \left[\frac{1}{\Delta t} [EM_{i,j}] K(\phi_{\alpha} w_{\alpha}^i)_j^{n+1} \right] \quad (9.2)$$

$$\{Am_{\alpha}^i\} = \sum_{\alpha} \sum_j \left[\frac{1}{\Delta t} [EM_{i,j}] K(\phi_{\alpha} S_{\alpha})_j^{n+1} + \sum_{id} \sum_{jd} \{d[ED]_{id,jd,i,j} K(\phi_{\alpha} S_{\alpha} D_{\alpha}^i)_j^{n+1}\} \right] \quad (9.3)$$

$$\{fh_{\alpha}^i\} = \sum_{\alpha} \sum_j \left[\frac{1}{\Delta t} [EM_{i,j}] \sum_{\beta} (\rho_{\beta} w_{\beta}^i S_{\beta\alpha})_j^n + \sum_{id} \sum_{jd} (\varepsilon - 1) [ED]_{id,jd,i,j} K(\rho_{\alpha} w_{\alpha}^i K_{\alpha})_j^n \right] (h_{\alpha,j})^n \\ - \sum_j \left[\sum_{jd} \left\{ [EK]_{jd,i,j} \left(\rho_{\alpha} w_{\alpha}^i K \frac{\partial \alpha}{\partial w} \right)_j \right\} + [EM_{i,j}] K(\phi_{\alpha} (t'_{\alpha} + s'_{\alpha}))_j \right] - \int W_{ib} q_{\alpha,d}^i dB - \int W_{ib} q_{\alpha,d}^i dB \quad (9.4)$$

$$\{fs_{\alpha}^i\} = \sum_{\alpha} \sum_j \left[\frac{1}{\Delta t} [EM_{i,j}] K(\phi_{\alpha} w_{\alpha}^i)_j^n (S_{\alpha,j})^n \right] \quad (9.5)$$

$$\{fm_{\alpha}^i\} = \sum_{\alpha} \sum_j \left[\frac{1}{\Delta t} [EM_{i,j}] K(\phi_{\alpha} w_{\alpha}^i)_j^n (S_{\alpha,j})^n + \sum_{id} \sum_{jd} (\varepsilon - 1) [ED]_{id,jd,i,j} K(\phi_{\alpha} S_{\alpha} D_{\alpha}^i)_j^n \right] (w_{\alpha,j}^i)^n \quad (9.6)$$

Using the above notation, equation (7) becomes

$$\sum_{\alpha=1}^{na} \{Ah_{\alpha}^i\} (h_{\alpha}) + \{As_{\alpha}^i\} (S_{\alpha}) + \{Am_{\alpha}^i\} (w_{\alpha}) = \{fh_{\alpha}^i\} + \{fs_{\alpha}^i\} + \{fm_{\alpha}^i\} \quad (10)$$

To reduce the computation time and to minimize the difficulties associated with the nonlinear terms, a decoupling technique is applied. The decoupling technique depends upon the property of each primary variable and is case specific. As an example, the governing equations of TCE migration are reduced to simplified forms with immobile air phase assumption, as follows :

The equation for water phase pressure head becomes :

$$[Ah_w^w] (h_w)^{n+1} = -[Ah_o^w] (h_o)^n + [Ah_w^w] (h_w)^n + \sum_{\alpha} \left\{ -[As_{\alpha}^w] (S_{\alpha})^n - [Am_{\alpha}^w] (w_{\alpha}^w)^n + \{fh_{\alpha}^w\}^n + \{fs_{\alpha}^w\}^n + \{fm_{\alpha}^w\}^n \right\} \quad (11.1)$$

The equation for oil phase pressure head of TCE becomes :

$$[Ah_o^o] (h_o)^{n+1} = -[Ah_w^o] (h_w)^{n+1} + [Ah_o^o] (h_o)^{n+1} + \sum_{\alpha} \left\{ -[As_{\alpha}^o] (S_{\alpha})^n - [Am_{\alpha}^o] (w_{\alpha}^o)^n + \{fh_{\alpha}^o\}^n + \{fs_{\alpha}^o\}^n + \{fm_{\alpha}^o\}^n \right\} \quad (11.2)$$

The equation for mass fraction of TCE component in the water phase becomes :

$$\sum_{\alpha} [Am_{\alpha}^0] (w_{\alpha}^0)^{n+1} = \sum_{\alpha} \left\{ -[Ah_{\alpha}^i] (h_{\alpha})^{n+1} - [As_{\alpha}^i] (S_{\alpha})^{n+1} + \{fh_{\alpha}^i\}^n + \{fs_{\alpha}^i\}^n + \{fm_{\alpha}^i\}^n \right\} \quad (11.3)$$

The element matrices were assembled in a banded form so that an asymmetric banded matrix solver can be used, which also reduces storage requirements for the variables. The assembled global matrix of three dimensional FEM is at least two orders of magnitude larger than two dimensional case; thus, an efficient matrix storage scheme and matrix solver are required. Either an asymmetric band matrix solver or a vector matrix solver [Pelka and Peters, 1986] for vector processing can be used. In this study, the Doolittle method was used for an asymmetric matrix solver [Pinder and Gray, 1977].

The system of equations is very dependent upon the component equations. To avoid a system of nonlinear algebraic equations, the nonlinear terms at the new (unknown) time level must be estimated. It is common practice to use the values of the nonlinear terms from the old time level. Iteration continues until the error criteria (difference of h_{α}^{n+1} , h_{α}^n and $w_{\alpha}^{i,n+1}$, $w_{\alpha}^{i,n}$) is satisfied. After each iteration, the computation proceeds to the next time level. Careful selection of the step size for space and time, and proper initial conditions, are required to reduce the instability problems related to nonlinearities [Abriola and Rathfelder, 1993]. To overcome the instability problems, it is necessary to use vari-

able time and spatial step sizes [Cooley, 1983]. The variable time step can be determined from the truncation error. The variable spatial step size requires the algorithm to find the sharp advancing front. The gradient of the concentration can indicate the presence of a sharp advancing front. Near this location, a smaller step size is required. In this study, mass lumping, upstream weighting, variable time step, advanced iteration techniques, and element-wise evaluation of parameters are used to avoid stability problems. If we construct the nodal points relations of each element in a fashion similar to the FDM, we can apply the methodology developed by Karplus [1958] to insure a stable solution. To provide a simple explanation, a stability analysis of a one-dimensional problem is implemented. Two- and three-dimensional cases and different basis functions, such as quadratic or Hermitian polynomials, can also be analyzed by expanding the following finite element analogue :

$$\begin{aligned} & \frac{1}{6\Delta t} \left[(C_{i+1}^{n+1} - C_{i+1}^n) + \alpha(C_i^{n+1} - C_i^n) + (C_{i-1}^{n+1} - C_{i-1}^n) \right] + \frac{V}{2\Delta x} \left[\alpha(C_{i+1} - C_{i-1})^{n+1} + (1-\alpha)(C_{i+1} - C_{i-1})^n \right] \\ & = \frac{D}{\Delta x^2} \left[\alpha(C_{i+1} - 2C_i + C_{i-1})^{n+1} + (1-\alpha)(C_{i+1} - 2C_i + C_{i-1})^n \right] \end{aligned} \quad (12)$$

Rearranging each term of the above equation in the form of $C_i^{n+1} - C_i^n$, the summation of all the coefficients should be less than 0 to satisfy the stability criteria.

$$\frac{D\Delta t}{\Delta x^2} = \frac{C_r}{P_e} \left(\frac{1}{3(1-\alpha)} \right) \quad (13)$$

Where, $C_r = V / (\Delta x / \Delta t)$ is the Courant number, and $P_e = V / (D / \Delta x)$ is the local Peclet number.

Because the system can be interpreted as the moving coordinate by the velocity component of the total derivative, the migration distance by convective flux should be within the already defined analogue. Therefore, $V / (\Delta x / \Delta t)$, which is same as $C_r(1)$.

The above FEM algorithm is very similar to the finite difference algorithm except for the time derivative, which is evaluated at three different spatial points with the weighting factors 1, 4, and 1. Applying the above technique to the generalized finite difference analogue, the stability condition of generalized FDM is as follows :

$$\frac{D\Delta t}{\Delta x^2} = \frac{C_p}{P_e} \left(\frac{1}{2(1-\theta)} \right) \quad (14)$$

The analogue of forward FEM and FDM is shown in Figure 1.

SIMULATION OF SPECIFIC PROBLEMS

1. Unsaturated Groundwater Flow

To demonstrate the robustness of the model to handle nonlinear problems, steady state drainage through an embankment was simulated [Cooley, 1983]. If capillary pressure is the dominant force of the system, then governing equation is simplified to equation (25) in Kim and Stenstrom [this issue]. And the problem was solved by the control parameters, such as the number of phases and dimensions, saturation values, and the mass fraction coefficients. The problem domain and data are shown in Figure 2 and Table 1.

The main difficulty of this simulation was the location of the unknown seepage height, which was determined using a moving, first-type boundary condition. Cooley's scheme [1983] was used to find the location. 175 iterations were required to satisfy the error criteria of 0.01 m. As shown in Figure 3, the result matches well with the results of Huyakorn et al. [1986].

2. Multiphase Flow System

If capillary pressure is the dominant force, then the governing equations for multiphase flow system are stated in (34.1) and (34.2). [Kim and Stenstrom, this issue]. By setting the number of dimension of the code as 1, 2, and 3, and mass fraction value of each phase as 0, the multidimensional capability of the code is displayed for multiphase flow. Problem domain and data are shown in Figure 4, and results are shown in Table 1. The accuracy of the model was verified by comparing the results of one-, two-, and three-dimensional problems for the case of zero flux boundary conditions. All three results show good agreement.

To observe the parameter dependency of the model in two-dimensional multiphase flow, the fluid conductivity was changed for several hypothetical cases. Problem domain and data are shown in Figure 5. As shown in Figure 6, the increased fluid conductivity enhanced the mobility of the phases at roughly one-to-one rate. The spatial derivative of fluid conductivity, dispersivity, velocity act like an advective flux, and numerical oscillation becomes a problem when the

spatial gradient of parameters is large, which causes convergence problems in the nonlinear iteration technique. The relative permeability depends upon the saturation; therefore, if the change of saturation is large, the relative permeability also causes a convergence problem. To insure rapid convergence, the residual saturation must be restricted. A value of 0.2 was used in this study. The constant head pressure boundary acts as a forcing pressure from the boundary. The river boundary of the water phase slowed the downward migration of the oil phase, and the resulting saturation profile of the oil phase is different from the conceptual model in Figure 6.

If the second-type boundary condition for the water phase flow is applied, the result of TCE migration is identical to conceptual model, as shown in Figure 7. The boundary condition should be selected carefully with respect to the location and characteristics. The best choice in this study seems to be the first-type, river boundary condition for the left side, and the second-type, flux boundary condition for the right side far away from contaminant source. Additional sensitivity analysis was implemented in the three-dimensional simulation of TCE for the boundary type, location, and the size of influx.

3. Composite Multiphase Contaminant Migration

Oil phase migration of a local contamination problem is slower relative to the case of an oil recovery problem. Thus, the capillary dominant approach is used. In composite multiphase flow, primary variables are pressure head and saturation, as shown in equation (22) of the accompanying paper [Kim and Stenstrom, this issue]. The result of saturation migration is shown in Figure 7.

In composite multiphase contaminant transport, the primary variables are the mass fraction of water and oil species in the water phase, as shown in equation (32) of the companion paper [Kim and Stenstrom, this issue]. The migration of mass fraction is shown in Figure 8 for two cases: (1) first-type boundary condition and large vertical fluid conductivity case, (2) second-type boundary condition and isotropic fluid conductivity case. As shown in Figure 8, the dissolved mass fraction of TCE is significant, which confirms empirical field observations that suggest transport of such compounds must be solved using a composite multiphase approach. Both the dissolved and immiscible TCE pose environmental problems. Since the water phase velocity is small compared to the velocity of the oil phase, the advective mass fraction flux does not cause a stability problem, and the movement of mass fraction depends upon the dispersive flux.

4. Three-Dimensional Simulation of TCE

Large scale three-dimensional simulations were implemented for TCE leachate from a hazardous landfill site to verify the integrated model against two-dimensional case using zero flux boundary condition along z direction. Three-dimensional grids are shown in Figure 9. The results of saturation migration are shown in Figure 10 for the same data as in two-dimensional problem with no flux boundary condition along z direction. The slight difference between Figures 7 and 10 is due to the plotting method, but the numerical results are identical for both cases. Sensitivity analyses are implemented with respect to the characteristics (Figure 11), the location of boundary conditions (Figure 12), the magnitude of the contaminant source (Figure 13) and the element size (Figure 12). As shown in Figure 11, the constant head pressure of the river boundary and inflow and outflow water fluxes acts as a forcing pressure from the boundary, hampering the downward migration of the oil phase. The apparent influence of the water inflow from the right side boundary is shown in Figure 11 and 13. Figure 12 shows the scale dependency of the model; the location of boundary condition has little effect upon the solution of the problem, which implies the applicability of moving boundary element method to NAPL problems [Stofoff and Pinder, 1992]. Increased size of the contaminant source slightly extends the migration profile along the horizontal direction. As shown in Figure 13, a 500% increase in the magnitude of contaminant source extends the TCE migration by approximately 250%.

The time-dependent migration patterns of TCE concentration in the water phase are shown in Figure 14 for the problem of (2) in Figure 13. The simulation is implemented for the unstable condition of the pressure head and the flow of each phase, caused from the river and source boundary condition to verify the model's stability criteria. Figure 12 shows no distinct unstable solution fluctuations.

CONCLUSIONS

A comprehensive finite element model was developed to solve the nonlinear transport and constitutive equations of the integrated groundwater model using multidimensional bilinear elements. The system of equations becomes singular at the interfacial region between different phases. To overcome this problem, hypothetical non-zero values of the saturation derivative and relative permeability are required for capillary dominant case. In this study, a saturation de-

rivative ranging from 10^{-4} to 10^{-5} was required. Steep spatial gradients of fluid conductivity and relative permeability cause greater numerical error, which requires more iterations, smaller time steps and spatial increments to control. The model is sensitive to the initial conditions of pressure head, saturation and mass fraction [Abriola and Rathfelder, 1993]. The rate of convergence is highly dependent upon the proper set of initial conditions. Due to the dependency of the saturation upon capillary pressure head, the constitutive equation between saturation and capillary head also effects the rate of convergence.

Contrary to many existing hypothetical simulation results, the first-type boundary conditions cannot be used to obtain results similar to the conceptual model. This is due to the fact that there should be a enough pressure build up of the oil phase to plunge downward to overcome the capillary pressure between the water and oil phases. For the field problems, it is appropriate to set the first-type boundary conditions far away from the contaminant source, or to use the second-type boundary conditions if there is no first-type boundary near.

Even though it was difficult to thoroughly optimize the code for vector processing due to the severe nonlinearities and the recursive relations among processes, the vectorization gave excellent results. The computation time after vectorization was only one third of the time required for scalar processing. The following programming techniques were used to facilitate vectorization.

1. The dimension of all arrays was defined in descending order ($A(np, ne, na)$, where $np > ne > na$).
2. About 80% of the computation time was spent in the evaluation of the element matrices. Therefore, the element matrices were evaluated over the whole domain, not over the each element, and assembled later. This facilitates vectorization, but increases the storage requirements.
3. In the case of multiple DO-loops, the inner-most DO-loop was for the largest array.
4. The recursive variables were evaluated outside of the DO-loops by using redundant variables.

The techniques presented in this study are very dependent upon the parameter values used in the simulation. Since many of the required parameters have never been measured in an actual groundwater basin, it is difficult to postulate the appropriate value and range of parameters. Large spatial gradients of fluid conductivity and relative permeability cause greater numerical error, which requires more iterations, smaller time steps and spatial increments, and more computation time. More extensive parameter analyses are in preparation and will be presented later in series papers.

Acknowledgments

This work was supported in part by National Science Foundation Engineering Research Center for Hazardous Substances Control, the UCLA Center for Risk and System Analysis for the Control of Toxics, and an environmental fellowship from BP-SOH10.

REFERENCES

- Abriola, L. M., and K. Rathfelder, Mass balance errors in modeling two-phase immiscible flows: causes and remedies, *Adv. in Water Res.*, 16, 223-239, 1993.
- Cooley, R. L., Some new procedure for numerical solution of variably saturated flow problems, *Water Resour. Res.*, 19(5), 1271-1285, 1983.
- Huyakorn, P. S., and K. Nikuha, Solution of transport equation using an upstream finite element scheme, *Appl. Math. Modeling*, 3, 7-17, 1979.
- Huyakorn, P. S., E. P. Springer, V. Guvanasen, and T. D. Wadsworth, A three-dimensional finite-element model for simulating water flow in variably saturated porous media, *Water Resour. Res.*, 22(13), 1790-1808, 1986.
- Kim, J.-H., Composite Multiphase Groundwater Model, Ph.D. thesis, University of California, Los Angeles, 1989.
- Kim, J.-H., and M. K. Stenstrom, An integrated groundwater model using multiphase multicomponent theory : 1. Theoretical Development, *This Issue*, 1995.
- Pelka, W., and A. Peters, Implementation of finite element groundwater for models on vector and parallel computers, VI International Conference on Finite Elements in Water Resources, Lisbon, Portugal, 301-312, 1986.
- Pinder, G. F., and W. G. Gray, *Finite Element Simulation in Surface and Subsurface Hydrology*, Academic Press Inc., 1977.
- Stofoff, S. A., G. F. Pinder, A boundary integral technique for multiple-front simulation of incompressible, immiscible flow in porous media, *Water Resour. Res.*, 28(8), 2067-2076, 1992.

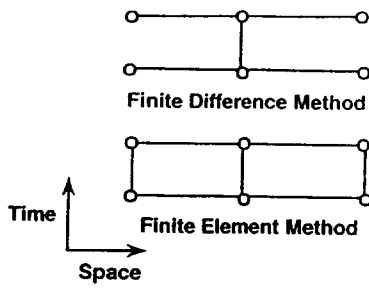


Figure 1. One Dimensional Analogs for F.E.M. and F.D.M..

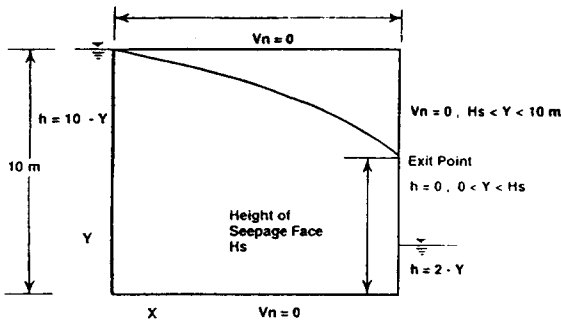


Figure 2. Problem definition of unsaturated seepage flow [Huyakorn et al., 1986a].

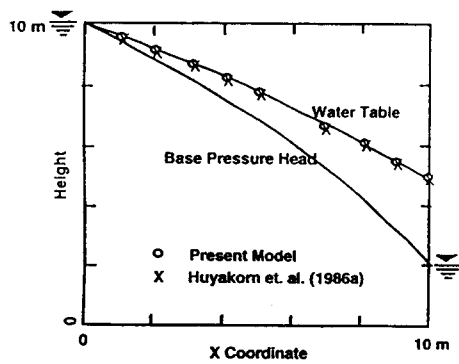


Figure 3. Groundwater table of unsaturated seepage flow.

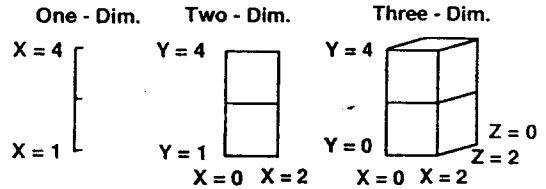


Figure 4. Dimensional representations of multiphase flow problem.

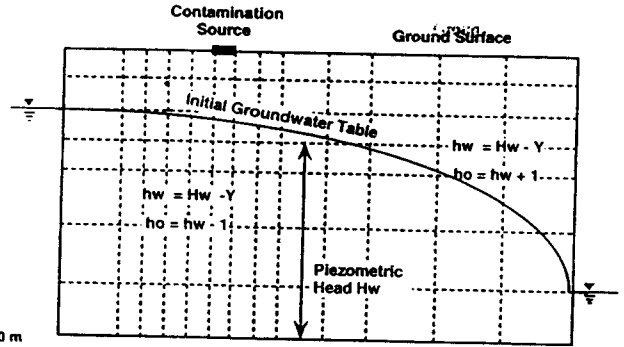
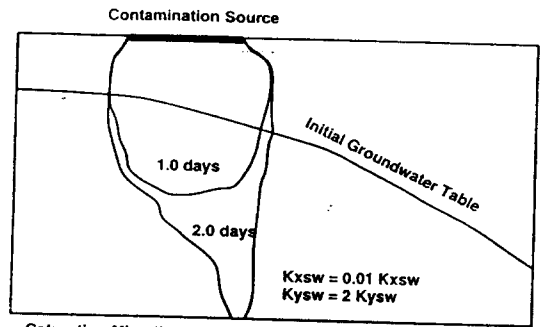
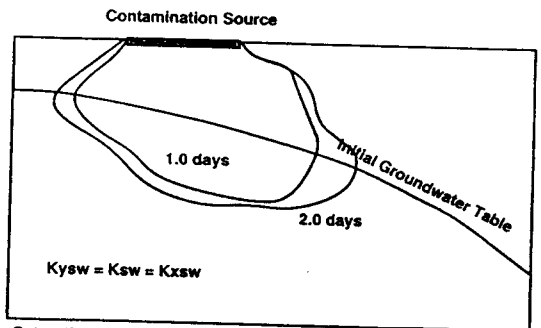


Figure 5. Finite element mesh, initial and boundary condition of composite multiphase flow.



Saturation Migration of TCE with 1st-type boundary condition.



Saturation Migration of TCE with 1st-type boundary condition.

Figure 6. Sensitivity of fluid conductivity and capillary pressure with 1st-type boundary condition.

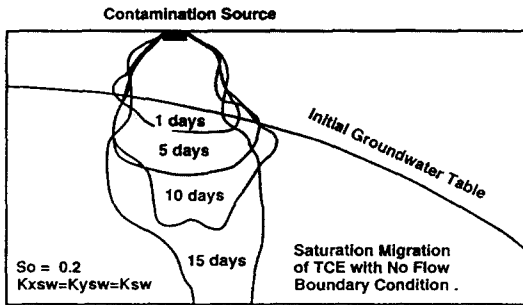
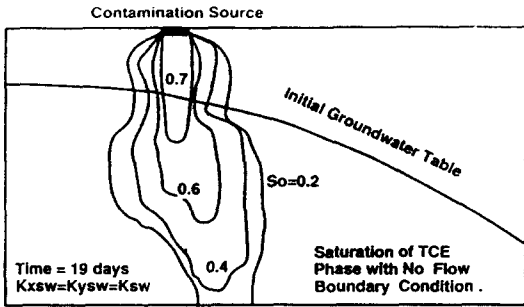


Figure 7. Saturation migration of TCE phase with no flow b. c. in homogeneous isotropic aquifer.

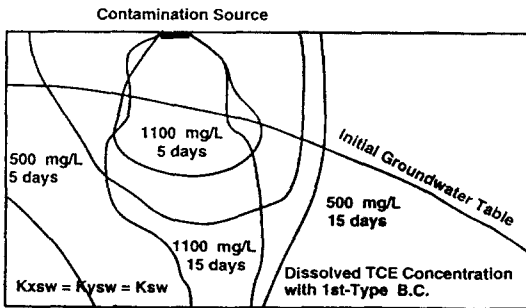
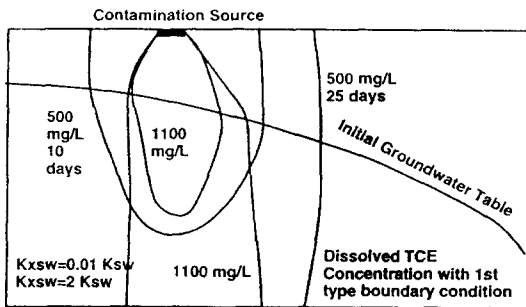


Figure 8. TCE Concentration in water phase with head and flow b. c. in iso- and anisotropic aquifer.

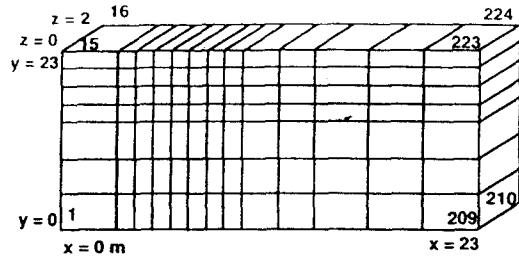


Figure 9. Three-dimensional finite element grids for composite multiphase flow.

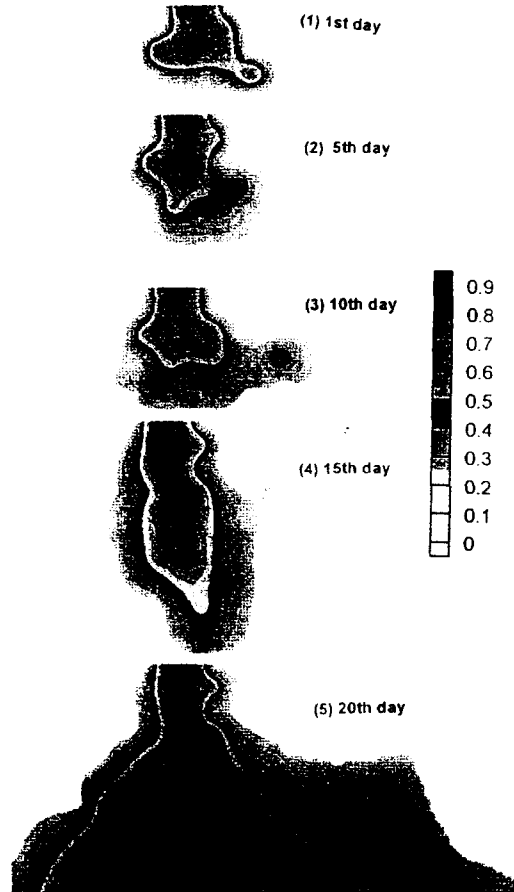


Figure 10. Three-dimensional saturation migration of TCE with no flow boundary conditions of water phase. (scale : $x = 23$ m, $y = 10$ m, $z = 2$ m)

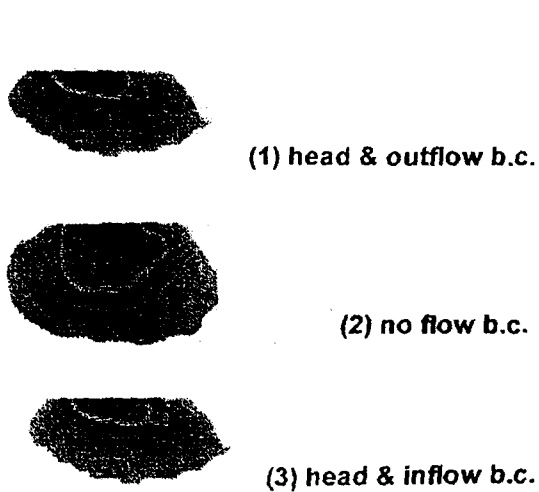


Figure 11. Sensitivity analysis of characteristic of boundary conditions. (scale : $x = 46$ m, $y = 10$ m , $z = 2$ m)

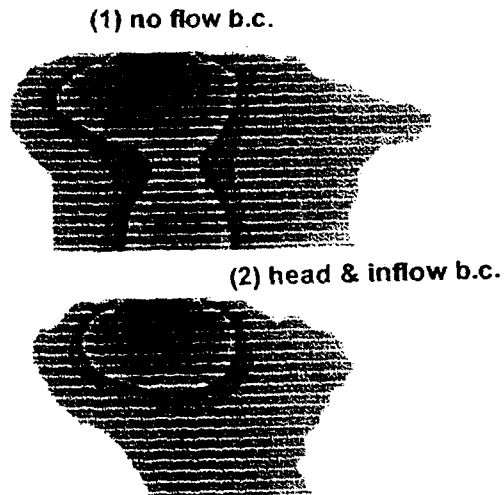


Figure 13. Magnitude effect of contaminant source (5 times larger than Figure 11.).

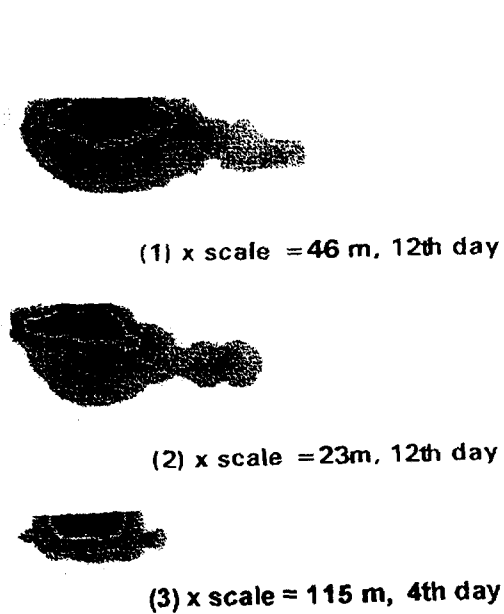


Figure 12. Scale effect of boundary region (head & inflow boundary conditions).

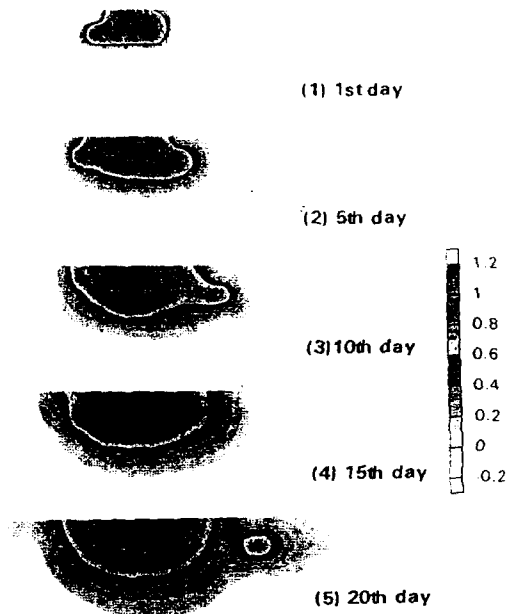


Figure 14. Migration of TCE concentration in water phase for problem (2) in Figure 13.

Table 1. Data of unsaturated seepage flow, multidimensional multiphase flow, and composite multiphase contaminant transport.

Parameters		Unsaturated Seepage Flow	Multidimensional Multiphase Flow	Composite Multiphase Contaminant Transport
Physical Data				
saturated conductivity	K_{sw}	0.01 m/day	1.008 m/day	0.5 m/day
pressure head of air phase	h_a	0.0 m	0.0 m	0.0 m
residual saturation	S_{rw}	0.2	0.2	0.2
saturation	S_{rt}	0.2	0.2	0.2
effective saturation of water phase	S_w^e	$1/(1+(\alpha_{ow}h_{aw})^n)$ for $h_{aw} > 0$ $\alpha_{ow} = 0.5623$ $n = 4$	$1/(1+(\alpha_{ow}h_{aw})^m)$ for $h_{aw} > 0$ $\alpha_{ow} = 5.2$ $n = 4, m = 1 - 1/n$	$1/(1+(\alpha_{ow}h_{aw})^m)$ for $h_{aw} > 0$ $\alpha_{ow} = 5.2$ $n = 4, m = 1 - 1/n$
effective saturation of total phase (oil + air phase)	S_t^e		$1/(1+(\alpha_{ow}h_{aw})^m)$ for $h_{aw} > 0$ $\alpha_{ow} = 11, \alpha_{ow} = 9.9$ $n = 4, m = 1 - 1/n$	$1/(1+(\alpha_{ow}h_{aw})^m)$ for $h_{aw} > 0$ $\alpha_{ow} = 11, \alpha_{ow} = 9.9$ $n = 4, m = 1 - 1/n$
water saturation	S_w	$S_{rw} + (S_{rt} - S_{rw})S_w^e$	$S_{rt} + (S_{rt} - S_{rw})S_w^e$	$S_{rt} + (S_{rt} - S_{rw})S_w^e$
oil saturation	S_o	$S_{rt} + (S_{rt} - S_{rt})S_w^e - S_w$	$S_{rt} + (S_{rt} - S_{rt})S_w^e - S_w$	$S_{rt} + (S_{rt} - S_{rt})S_w^e - S_w$
air saturation	S_a		$1 - S_t$	$1 - S_t$
water relative permeability	k_{rw}	$(S_w^e)^m$ $m = 4$	$(S_w^e)^{1/2}$ $[1 - (1 - S_w^e)^{1/m}]^2$	$(S_w^e)^{1/2}$ $[1 - (1 - S_w^e)^{1/m}]^2$
oil relative permeability	k_{ro}		$(S_o^e S_w^e)^{1/2} [(1 - S_w^e)^{1/m}]^m$ $- (1 - S_o^e)^{1/2} [(1 - S_w^e)^{1/m}]^2$	$(S_o^e S_w^e)^{1/2} [(1 - S_w^e)^{1/m}]^m$ $- (1 - S_o^e)^{1/2} [(1 - S_w^e)^{1/m}]^2$
Numerical Data				
spatial step size		$\Delta x = \Delta y = 1$ m	$\Delta x = 2, \Delta y = 2, \Delta z = 2$ m	variable size
error criteria		0.01 m	0.1 m	0.01 m
weighting factor		$f_{D_{xy}} = 0.1, f_{D_z} = 0.68$	$f_{D_{xy}} = 0.1, f_{D_z} = 0.68$	$f_{D_{xy}} = 0.1, f_{D_z} = 0.68$

Table 2. Data of multidimensional multiphase flow, and composite multiphase contaminant transport.

Parameters		Multidimensional Multiphase Flow	Composite Multiphase Contaminant Transport
Physical Data			
longitudinal dispersivity			$\alpha_x = 0.5574, \alpha_y = 0.2784, \alpha_z = 1.0034$
solubility limit	H^*		1100 ppm
viscosity ratio	μ_{ro}	0.5	0.5
density ratio	ρ_{ro}	1.2	1.2
initial conditions		1-dim: $h_w = 2 - x, h_o = h_w - 0.3$ 2-dim: $h_w = 2 - y, h_o = h_w - 0.3$ 3-dim: $h_w = 2 - y, h_o = h_w - 0.3$	unsaturated region: $h_w = H_w - y, h_o = h_w + 1$ saturated region: $h_w = H_w - y, h_o = h_w - 1$ H_w : height of initial groundwater table
boundary conditions		1-dim: at $x = 0, h_w = 2, (\partial h_w) / (\partial x) = 0$, at $x = 4, h_w = 0.01, (\partial h_w) / (\partial x) = 0$ 2-, 3-dim: at $y = 0, h_w = 2, (\partial h_w) / (\partial y) = 0$, at $y = 4, h_w = 0.01, (\partial h_w) / (\partial y) = 0$	$x = 0: h_w = 8 - y, h_o = h_w - 1$ $x = 4: h_w = 2 - y, h_o = h_w - 1$

Table 3. Multidimensional multiphase flow results of TCE.

	$x = 0$	$x = 0$	$x = 0$	$x = 0$	$x = 2$	$x = 2$	$x = 2$
	1-dim.	2-dim.	3-dim.	3-dim.	2-dim.	3-dim.	3-dim.
	$z = 0$	$z = 0$	$z = 0$	$z = 2$	$z = 0$	$z = 0$	$z = 2$
Time =	0.01	0.01	0.01	0.01	0.01	0.01	0.01
$y = 4$	0.77	0.77	0.77	0.77	0.77	0.77	0.77
$y = 2$	0.20	0.20	0.20	0.20	0.20	0.20	0.20
$y = 0$	0.20	0.20	0.20	0.20	0.20	0.20	0.20
Time =	0.0504	0.0504	0.0504	0.0504	0.0504	0.0504	0.0504
$y = 4$	0.77	0.77	0.77	0.77	0.77	0.77	0.77
$y = 2$	0.21	0.23	0.27	0.27	0.23	0.27	0.27
$y = 0$	0.20	0.20	0.20	0.20	0.20	0.20	0.20
Time =	0.1074	0.1074	0.1074	0.1074	0.1074	0.1074	0.1074
$y = 4$	0.77	0.77	0.77	0.77	0.77	0.77	0.77
$y = 2$	0.26	0.33	0.40	0.40	0.33	0.40	0.40
$y = 0$	0.20	0.20	0.20	0.20	0.20	0.20	0.20